Narrow band exciton coupled with acoustical anharmonic phonons: application to the vibrational energy flow in a lattice of H-bonded peptide units

2009 J. Phys.: Condens. Matter 21 185404

(http://iopscience.iop.org/0953-8984/21/18/185404)

IOP Publishing Journal of Physics: Condensed Matter

J. Phys.: Condens. Matter **21** (2009) 185404 (15pp) doi:10.1088/0953-8984/21/18/185404

Narrow band exciton coupled with acoustical anharmonic phonons: application to the vibrational energy flow in a lattice of H-bonded peptide units

Vincent Pouthier

Institut UTINAM, UMR CNRS 6213, Université de Franche-Comté, F-25030 Besançon Cedex, France

E-mail: vincent.pouthier@univ-fcomte.fr

Received 10 November 2008, in final form 18 March 2009
Published 6 April 2009
Online at stacks.iop.org/JPhysCM/21/185404

Abstract

A time-convolutionless master equation is established for describing the transport properties of amide-I vibrons coupled with acoustic phonons in a lattice of H-bonded peptide units. Within the non-adiabatic weak coupling limit, it is shown that the vibron dynamics strongly depends on the nature of the phonons and two distinct mechanisms have been identified. Harmonic phonons, which support spatial correlations over an infinite length scale, induce a fast dephasing–rephasing mechanism in the short time limit. Consequently, the vibron keeps its wavelike nature and a coherent vibrational energy flow takes place whatever the temperature. By contrast, anharmonic phonons carry spatial correlations over a finite length scale, only. As a result, the rephasing process no longer compensates the dephasing mechanism so that dephasing-limited band motion occurs. It gives rise to the incoherent diffusion of the vibron characterized by a diffusion coefficient whose temperature dependence scales as $1/T^{\alpha}$. In the weak anharmonicity limit, the exponent α is about 2. It becomes smaller than unity in the strong anharmonicity limit, indicating that the diffusion coefficient behaves as a slowly decaying function of the temperature.

(Some figures in this article are in colour only in the electronic version)

1. Introduction

In a recent series of papers, a small polaron approach has been used to describe how narrow band excitons may promote vibrational energy flow in a lattice of H-bonded peptide units [1–5]. These works were based on the seminal model introduced by Davydov and Kisluka [6], and later by Scott [7], to describe bioenergy transport in α-helices in terms of a soliton mechanism. The main idea is that the energy is transferred by amide-I vibrations (C=O stretching modes) which delocalize due to dipole–dipole coupling and give rise to vibrational excitons called vibrons. Since each C=O group is engaged in an H bond, the vibrons interact with the phonons describing the H-bond network dynamics. By assuming that the phonons behave in a classical way, the strong vibron–phonon coupling is responsible for a nonlinear dynamics which counterbalances the dispersion created by the dipole–dipole interaction. Therefore a vibron propagates according to the so-called Davydov soliton which provides an approximation to the self-trapping phenomena. Soliton mechanisms for bioenergy transfer in proteins have received increasing attention during the last three decades and a broad review can be found in [8–10].

Nevertheless, it has been suggested that the solution to the Davydov problem is rather a small polaron than a soliton [11–16]. Indeed, in a lattice of H-bonded peptide units, the vibron bandwidth is smaller than the phonon cutoff frequency. The non-adiabatic limit is reached so that the quantum nature of the phonons plays a crucial role. During its propagation, a vibron is dressed by a virtual cloud of phonons that corresponds to a contraction of the H bonds surrounding the excited site. The dressed vibron forms a small polaron.

From a theoretical point of view, a fully or partially dressed vibron basis is obtained by performing a modified Lang–Firsov (MLF) transformation [17]. It is defined in terms of temperature-dependent variational parameters whose optimization is achieved by using thermodynamic arguments [16, 18]. From the estimated value of the coupling strength (the so-called χ parameter) [8–10], partially dressed vibrons are expected to occur at low temperatures whereas fully dressed vibrons must take place at biological temperatures. However, MLF is not exact due to the delocalized nature of the vibrons and a polaron–phonon coupling remains. It is responsible for relaxation and gives rise to the incoherent diffusive motion of the small polarons (see, for instance, [2, 19–22]).

Although the small polaron formalism provides a powerful tool to describe energy flow in proteins, its usefulness, when compared with other methods, requires first the vibron–phonon coupling to be stronger than the vibron bandwidth and, second, the acoustic phonons to be harmonic. However, the physical relevance of these two conditions is clearly questionable in realistic systems.

Indeed, most of the works devoted to the Davydov problem involve χ values extracted from an indirect and uncertain comparison between experimental and theoretical results. However, estimations of the coupling strength have been carried out by performing *ab initio* calculations for the formamide dimer, i.e. the smallest model of an α-helix fragment containing two H-bonded peptide units [23–25]. It has been shown that most *ab initio* estimates yield smaller χ values, often negative, when compared with the usually admitted χ values. Indeed, in its pioneering calculations, Kuprievich found a χ value equal to -33 and -17 pN, respectively, depending on whether the anharmonicity of the amide-I mode is considered or not [23]. More recently, Pierce has shown that χ is either equal to -7 or $+26$ pN, depending on the geometry of the dimer [24]. Finally, when the two molecules were forced into a geometry that approximates two H-bonded peptide units in an α-helix, Ostergard obtained rather weak χ values of about -7.55 pN [25].

Moreover, especially at biological temperatures, the peptide units are expected to develop large amplitude motions so that they may be able to explore regions located more or less far from their equilibrium position. Since the H bond is usually considered as a relatively weak interaction, we expect the peptide units to be rather sensitive to the anharmonicity of the potential energy. Consequently, the harmonic approximation certainly fails in describing the H-bond dynamics. The acoustic phonons have a finite lifetime and their extended nature disappears [26–29].

In the present paper, the vibrational energy flow in a lattice of H-bonded peptide units is revisited within the non-adiabatic weak coupling limit. The phonons are assumed to form a thermal bath and special attention is paid to characterize the influence of their anharmonicity on the vibron dynamics. It will be shown that, for harmonic phonons, spatial correlations over an infinite length scale occur in the bath. They prevent dephasing so that the vibron delocalizes coherently along the lattice in spite of its coupling with the phonons. By contrast, anharmonic phonons carry spatial correlations over a finite length scale. Consequently, a transition between a coherent (wavelike) motion in the short time limit and an incoherent (diffusion-like) motion in the long time limit takes place. To study these features, a bare vibron basis is used and a standard perturbation theory is applied. A generalized master equation (GME) for the vibron reduced density matrix (RDM) is established by using the so-called time-convolutionless (TCL) approach. It allows a systematic analysis of non-Markovian effects and it gives a better approximation to the exact solution than standard methods [30–35].

This paper is organized as follows. In section 2, a modified Davydov model is first introduced to account for the anharmonic nature of the phonons. Then, the weak coupling limit is discussed and the key observables required to study the transport properties are introduced. In section 3, the GME for the vibron RDM is established and the vibron time-dependent diffusion coefficient is defined. The diffusion coefficient is evaluated numerically in section 4 where a detailed analysis of the energy transfer is performed. Finally, these results are interpreted in section 5.

2. Description of the system

2.1. Model Hamiltonian

In a 1D lattice of H-bonded peptide units, each site $x = 1, \ldots, N$ contains an amide-I mode with frequency ω_0. Restricting our attention to the one-vibron dynamics, the xth amide-I mode is equivalent to a two-level system whose first excited state is denoted $|x\rangle$. The zero-vibron state, defined as the vacuum state $|\oslash\rangle$, describes all the amide-I modes in their ground state. The vibron Hamiltonian is thus written as (in units $\hbar = 1$)

$$H_{\rm v} = \sum_x \omega_0 |x\rangle\langle x| + \Phi[|x+1\rangle\langle x| + |x\rangle\langle x+1|] \quad (1)$$

where Φ is the vibron hopping constant. This Hamiltonian describes narrow band excitons which delocalize along the lattice according to plane waves with wavevector K and eigenfrequency $\omega_K = \omega_0 + 2\Phi\cos(K)$. This propagation is accounted by the free propagator $G(t) = \exp(-{\rm i}H_{\rm v}t)$, whose matrix elements are defined in terms of the Bessel function of the first kind $J_n(z)$ as

$$G_{xx'}(t) = (-{\rm i})^{(x-x')} {\rm e}^{-{\rm i}\omega_0 t} J_{x-x'}(2\Phi t). \quad (2)$$

The vibrons interact with the external motions of the peptide units which result from the collective dynamics of the H-bond network. The xth peptide unit, with mass M, performs a small displacement u_x around its equilibrium position. It interacts with its two neighboring units via pairwise intermolecular potentials. By expanding these potentials around equilibrium to third order with respect to displacements, the H-bond dynamics is governed by the Hamiltonian $H_{\rm p}$ defined as

$$H_{\rm p} = \sum_x \frac{p_x^2}{2M} + \frac{W}{2}(u_{x+1} - u_x)^2 - \frac{\delta}{6}(u_{x+1} - u_x)^3 \quad (3)$$

where p_x is the momentum connected to u_x and where W and δ denote the quadratic and the cubic H-bond force constants, respectively.

In the present approach, the H-bond anharmonicity is assumed to be sufficiently small so that a standard perturbation theory can be applied. Therefore, only the cubic anharmonicity is considered although high-order contributions may be included in a straightforward way. In that case, the harmonic part of H_p defines standard phonons which correspond to a set of N low frequency acoustic modes labeled by the wavevector q and described by the boson operators $a_q^\dagger$ and a_q. The harmonic frequency of the qth phonon is defined as $\Omega_q = \Omega_\mathrm{c}\sin(q/2)$, where $\Omega_\mathrm{c} = \sqrt{4W/M}$ is the phonon cutoff frequency. Consequently, the H-bond network Hamiltonian can be rewritten as $H_\mathrm{p} = \sum_q \Omega_q a_q^\dagger a_q + V$, where the phonon–phonon interaction V is easily expressed in terms of the phonon operators [29].

According to the potential deformation model, the vibron–phonon interaction results from a random modulation of the internal frequency of each amide-I mode by the peptide unit motions as

$$\Delta H = \sum_{xq} (\Delta_{qx} a_q^\dagger + \Delta_{qx}^* a_q)|x\rangle\langle x| \tag{4}$$

where $\Delta_{qx} = -\mathrm{i}\Delta_0 \sin(q)/\sqrt{|\sin(q/2)|}\mathrm{e}^{-\mathrm{i}qx}/\sqrt{N}$ involves the χ parameter introduced by Davydov as $\Delta_0 = \chi(\hbar^2 MW)^{-1/4}$ ($\hbar$ has been reintroduced to avoid confusion).

Finally, the vibron–phonon dynamics is governed by the full Hamiltonian $H = H_\mathrm{v} + H_\mathrm{p} + \Delta H$ which will be used to study the vibron transport properties. This Hamiltonian slightly differs from the original Davydov model in which the harmonic approximation has been invoked to define the phonon Hamiltonian. In the present approach, as shown in the last term in the right-hand side of equation (3), the phonons no longer represent independent excitations due to the anharmonic nature of the potential that links two neighboring peptide units. Moreover, in a marked contrast with previous works, we shall assume that the vibron–phonon coupling represents a small perturbation. The validity of this approximation is thus discussed in section 2.2.

2.2. Validity of the weak coupling limit

The vibron dynamics originates from the competition between the hopping constant, which measures the ability of the vibron to delocalize coherently, and the vibron–phonon interaction, which favors a diffusion-like motion. To estimate the relevance of these two mechanisms, let us suppose that the system is initially prepared in the state $|x, \{n_q\}\rangle$. It describes the xth amide-I mode in its first excited state whereas the lattice is in a well-defined number state involving n_q phonons in each mode q.

On the one hand, the coupling ΔH (4) leading to fluctuations in the phonon numbers, $|x, \{n_q\}\rangle$, decays into the energy continuum formed by the phonon bath. It thus acquires a finite width whose value is given by the corresponding decay rate 2Γ. By assuming the phonons are harmonic and in thermal equilibrium at temperature T, a second-order perturbation theory yields $\Gamma = 8E_\mathrm{B}k_\mathrm{B}T/\Omega_\mathrm{c}$ (k_B is the Boltzmann constant) where $E_\mathrm{B} = 2\Delta_0^2/\Omega_\mathrm{c}$ is the small polaron binding energy. On the other hand, due to dipole–dipole coupling, $|x, \{n_q\}\rangle$ interacts with neighboring states $|x \pm 1, \{n_q\}\rangle$. This gives rise to a band around ω_0 whose width is equal to 4Φ.

Consequently, the weak coupling limit will be reached if the width of each local state 2Γ is smaller than the vibron bandwidth 4Φ. By using typical values for the parameters defining the Davydov model, i.e. $\Phi = 7.8\ \mathrm{cm}^{-1}$, $W = 15\ \mathrm{N\ m}^{-1}$ and $M = 1.8 \times 10^{-25}$ kg, this condition is satisfied at biological temperatures ($T = 310$ K) provided that $|\chi| < 16.16$ pN (i.e. $E_\mathrm{B} < 0.87\ \mathrm{cm}^{-1}$). Therefore, the small $|\chi|$ values calculated by Pierce and Ostergard [24, 25] clearly suggest that the dipole–dipole coupling predominates over the vibron–phonon interaction, even at biological temperatures. It is thus natural to address the vibron transport properties by using a bare vibron basis rather than a dressed vibron basis, as illustrated in the following sections.

2.3. Transport properties

Without any perturbation, the lattice of H-bonded peptide units is in thermal equilibrium at temperature T at least equal to the biological temperature. Since $\omega_0 \approx 1660\ \mathrm{cm}^{-1}$, each amide-I mode lies in its ground state. This is no longer the case for the phonons ($\Omega_\mathrm{c} \approx 100\ \mathrm{cm}^{-1}$) whose eigenstates are not well defined. A statistical average is thus required by using the Boltzmann distribution ρ_p for the phonon density matrix. Therefore, to study the vibrational energy flow we assume that the lattice reaches a configuration out of equilibrium. We suppose that a vibron is created on the site $x_0 = 0$ so that the initial density matrix is $\rho = \rho_\mathrm{v} \otimes \rho_\mathrm{p}$, where $\rho_\mathrm{v} = |x_0\rangle\langle x_0|$. Note that such an excitation may result from the energy released by the hydrolysis of ATP [6] or from charge neutralization upon electron capture by a protonated α-helix [1].

To characterize the vibrational energy flow, let the vibron density $P(x,t)$ define the average vibron number on the xth site at time t as

$$P(x,t) = \mathrm{Tr}[\rho \mathrm{e}^{\mathrm{i}Ht}|x\rangle\langle x|\mathrm{e}^{-\mathrm{i}Ht}]. \tag{5}$$

In principle, the knowledge of $P(x,t)$ yields all the required observables to describe the energy redistribution. Among the different observables, we shall focus our attention on the time-dependent diffusion coefficient defined in terms of the vibron mean square displacement as

$$D(t) = \frac{1}{2}\left(\frac{\mathrm{d}\langle x^2(t)\rangle}{\mathrm{d}t}\right). \tag{6}$$

The time evolution of $D(t)$ gives fundamental information on the vibron dynamics. Indeed, a linear dependence of $D(t)$ with respect to time indicates a coherent energy transfer resulting from a wavelike motion of the vibron. By contrast, $D(t)$ becomes time-independent when an incoherent diffusive regime takes place and it vanishes when energy localization occurs.

At this step, a complete characterization of the diffusion coefficient required the knowledge of a more general object, namely the vibron RDM $\sigma(t)$, defined as

$$\sigma(x_1, x_2, t) = \mathrm{Tr}[\rho \mathrm{e}^{\mathrm{i}Ht}|x_2\rangle\langle x_1|\mathrm{e}^{-\mathrm{i}Ht}]. \tag{7}$$

The RDM describes the vibron state at time t after performing an average over the phonon bath. Diagonal elements yield the vibron density whereas non-diagonal elements measure the coherence between local states. Under the influence of H, diagonal and non-diagonal elements mix in a complex manner so that the time evolution of the full RDM must be studied to extract the information that is desired.

3. Time-convolutionless GME and diffusion coefficient

3.1. Time-convolutionless GME

To determine the GME for the vibron RDM, we use the standard projector method of the TCL approach [30–35] which has been successfully applied to characterize small polaron dynamics in α-helices [1–3]. Therefore, by performing a second-order expansion with respect to ΔH, the GME is expressed as

$$\begin{aligned}\mathrm{i}\dot{\sigma}(x_1,x_2,t) &= \Phi\sum_{s=\pm1}[\sigma(x_1+s,x_2,t)-\sigma(x_1,x_2+s,t)]\\ &\quad-\mathrm{i}\sum_{\bar{x}_1,\bar{x}_2}\mathcal{J}(x_1,x_2,\bar{x}_1,\bar{x}_2,t)\sigma(\bar{x}_1,\bar{x}_2,t).\end{aligned}\tag{8}$$

The first term in the right-hand side of equation (8) describes the coherent dynamics under the influence of the vibron Liouvillian $\mathcal{L}_\mathrm{v}=[H_\mathrm{v},\ldots]$. By contrast, the influence of the bath is characterized by the relaxation operator $\mathcal{J}(t)$ whose matrix elements are written as

$$\begin{aligned}\mathcal{J}(x_1,x_2,\bar{x}_1,\bar{x}_2,t) &= [\Gamma_{x_1\bar{x}_1}(t)-W_{x_1\bar{x}_1,x_2}(t)]\delta_{x_2,\bar{x}_2}\\ &\quad+[\Gamma^*_{x_2\bar{x}_2}(t)-W^*_{x_2\bar{x}_2,x_1}(t)]\delta_{x_1,\bar{x}_1}.\end{aligned}\tag{9}$$

In equation (9), $\Gamma(t)$ and $W(t)$ involve both the vibron–phonon coupling correlation function $C_{x_1,x_2}(\tau)=\langle\Delta H_{x_1x_1}(\tau)\Delta H_{x_2x_2}(0)\rangle$ and the free vibron propagator (2) as

$$\begin{aligned}\Gamma_{x_1\bar{x}_1}(t) &= \sum_x\int_0^t \mathrm{d}\tau\, C_{x_1,x}(\tau)G_{x_1,x}(\tau)G^*_{\bar{x}_1,x}(\tau)\\ W_{x_1\bar{x}_1,x_2}(t) &= \sum_x\int_0^t \mathrm{d}\tau\, C_{x_2,x}(\tau)G_{x_1,x}(\tau)G^*_{\bar{x}_1,x}(\tau).\end{aligned}\tag{10}$$

Note that the operators occurring in $C_{x_1,x_2}(\tau)$ depend on the phonon degrees of freedom only. Their time dependence results from a Heisenberg representation with respect to H_p and the symbol $\langle\cdots\rangle$ denotes an average over the phonon bath.

The GME is isomorphic to the Schrödinger equation for a single particle moving on a 2D lattice [2]. This lattice is a graphical representation of the Liouville space in which the site position is defined by the two indexes (x_1,x_2). The RDM plays the role of a wavefunction whose dynamics is governed by the time-dependent effective Liouvillian $\mathcal{L}_\mathrm{v}-\mathrm{i}\mathcal{J}(t)$. Within this equivalence, $\mathcal{L}_\mathrm{v}$ gives rise to an anisotropic dynamics which is translationally invariant along the directions x_1 and x_2. However, a symmetry breaking is induced by $\mathcal{J}(t)$ which accounts for the dephasing mechanism and describes both coherence decays and coherence transfers. Note that the vibron–phonon coupling (4) does not affect the vibron hopping constant. Incoherent hops between neighboring sites are forbidden to second order so that $\mathcal{J}(x,x,\bar{x}_1,\bar{x}_2,t)=0,\forall x$.

Nevertheless, both $G_{x_1,x_2}(t)$ and $C_{x_1,x_2}(t)$ depend on the distance $|x_1-x_2|$ (see the appendix). Therefore $\mathcal{J}(x_1,x_2,\bar{x}_1,\bar{x}_2,t)$ is a function of x_1-x_2, $\bar{x}_1-\bar{x}_2$, $\bar{x}_2-x_2$ and $\bar{x}_1-x_1$ only. The 2D Liouville space remains translationally invariant along the direction $x_1=x_2$. Consequently, $\sigma(x_1,x_2,t)$ only depends on x_1 and $r=x_2-x_1$ and it can be expanded as a Bloch wave as [2, 36]

$$\sigma(x_1,x_1+r,t)=\frac{1}{N\mathrm{i}^r}\sum_k\Psi_k(r,t)\mathrm{e}^{-\mathrm{i}k(x_1+r/2)}.\tag{11}$$

The momentum k, which takes N values in the first Brillouin zone of the lattice, describes the RDM delocalization along the direction $x_1=x_2$. Since k is a good quantum number, the effective Liouvillian is block diagonal and the GME can be solved for each k value as

$$\begin{aligned}\mathrm{i}\dot{\Psi}_k(r,t) &= \Phi_k\sum_{s=\pm1}\Psi_k(r+s,t)\\ &\quad-\mathrm{i}\sum_{\bar{r}}\mathcal{J}_k(r,\bar{r},t)\Psi_k(\bar{r},t)\end{aligned}\tag{12}$$

where $\Phi_k=2\Phi\sin(k/2)$ and where the matrix elements of $\mathcal{J}_k(t)$ are defined as

$$\begin{aligned}\mathcal{J}_k(r,\bar{r},t) &= 2\mathrm{i}^{r-\bar{r}}\,\mathrm{Re}\sum_h\mathrm{e}^{-\mathrm{i}k(r-\bar{r})/2}\int_0^t\mathrm{d}\tau C_{0h}(\tau)\\ &\quad\times[G_{0,h}(\tau)G^*_{0,r-\bar{r}+h}(\tau)-G_{0,r+h}(\tau)G^*_{0,\bar{r}+h}(\tau)].\end{aligned}\tag{13}$$

The resulting GME (12) is isomorphic to the Schrödinger equation for a single particle moving on a 1D lattice. It can be expressed in a formal way since $\Psi_k(r,t)$ can be viewed as the component of the vector $|\Psi_k(t)\rangle$ in the site representation $\{|r\rangle\}$. At time $t=0$, the vibron creation on the site $x_0=0$ yields $|\Psi_k(0)\rangle=|0\rangle,\forall k$. The evolution of $|\Psi_k(t)\rangle$ is thus governed by a Schrödinger-like equation as

$$\mathrm{i}|\dot{\Psi}(t)\rangle=\mathcal{H}_k(t)|\Psi(t)\rangle\tag{14}$$

where the matrix elements of the effective Hamiltonian $\mathcal{H}_k(t)$ are defined as

$$\mathcal{H}_k(r,\bar{r},t)=\Phi_k(\delta_{r,\bar{r}+1}+\delta_{r,\bar{r}-1})-\mathrm{i}\mathcal{J}_k(r,\bar{r},t).\tag{15}$$

3.2. Diffusion coefficient: general expression

The formal expression of the time-dependent diffusion coefficient (6) can be extracted from the GME (14) without explicitly solving this master equation. To proceed, the starting point is to express the vibron mean square displacement as (see (11))

$$\langle x^2(t)\rangle=-\left(\frac{\partial^2\langle 0|\Psi_k(t)\rangle}{\partial k^2}\right)_{k=0}.\tag{16}$$

Then, let $\mathcal{U}_k(t)$ denote the evolution operator associated with the Schrödinger-like equation (14). It connects the vector $|\Psi_k(t)\rangle$ to its initial value, i.e. $|\Psi_k(t)\rangle=\mathcal{U}_k(t)|0\rangle$, and it satisfies $\mathcal{U}_k(0)=1$. Its time evolution is governed by the equation $\mathrm{i}\dot{\mathcal{U}}_k(t)=\mathcal{H}_k(t)\mathcal{U}_k(t)$. Therefore, it is straightforward to show that $D(t)$ involves the second derivative with respect

to k of $\langle 0|\mathcal{H}_k(t)\mathcal{U}_k(t)|0\rangle$. Since (13) yields $\mathcal{J}_k(0,\bar{r},t) = 0$, $\forall\bar{r}$, $\langle 0|\mathcal{H}_k(t)$ only involves the time-independent part of $\mathcal{H}_k(t)$ (15). As a result, after simple algebraic manipulations, $D(t)$ is finally expressed as

$$D(t) = \mathrm{i}\Phi \sum_{r=\pm 1}\left(\frac{\partial\langle r|\mathcal{U}_k(t)|0\rangle}{\partial k}\right)_{k=0}. \tag{17}$$

Equation (17) reveals that the time evolution of $D(t)$ is governed by the long-wavelength behavior of the evolution operator. This behavior can be extracted from (14) by applying a standard perturbation theory in which k is assumed to be a small parameter. To proceed, the effective Hamiltonian is expanded as

$$\mathcal{H}_k(t) = \mathcal{H}_0(t) + k\mathcal{H}_0'(t) + \frac{k^2}{2}\mathcal{H}_0''(t) + \cdots \tag{18}$$

where the prime denotes a derivative with respect to k and where the index 0 means that the operators are evaluated for $k = 0$. From (18), the expansion of $\mathcal{U}_k(t)$ in a power series with respect to k can be easily reached and one finally obtains

$$D(t) = \Phi \sum_{r=\pm 1}\int_0^{t_1} \mathrm{d}t_1 \langle r|\mathcal{G}(t,t_1)\mathcal{H}_0'(t_1)\mathcal{G}(t_1,0)|0\rangle \tag{19}$$

where $\mathcal{G}(t_1,t_2) = \mathcal{U}_0(t_1)\mathcal{U}_0^{-1}(t_2)$ is expressed in terms of the unperturbed evolution operator $\mathcal{U}_0(t)$ connected to $\mathcal{H}_0(t)$, i.e. $\dot{\mathcal{U}}_0(t) = -\mathcal{J}_0(t)\mathcal{U}_0(t)$.

From (15), $\mathcal{H}_0'(t)$ exhibits two contributions. The first contribution is proportional to Φ whereas the second contribution involves $\mathcal{J}_0'(t)$. As a consequence, the diffusion coefficient is expressed as the sum of two terms, i.e. $D(t) = D_{\mathrm{B}}(t) + D_{\mathrm{C}}(t)$. The coefficient $D_{\mathrm{B}}(t)$, proportional to Φ^2, defines the band diffusion coefficient which basically accounts for dephasing-limited band motion. By contrast, $D_{\mathrm{C}}(t)$ is the cross-diffusion coefficient proportional to both Φ and $\mathcal{J}_0'(t)$. These two terms are thus defined as

$$\begin{aligned} D_{\mathrm{B}}(t) &= \sum_{r=\pm 1}\sum_{r_1 r_2}\int_0^{t_1}\mathrm{d}t_1\,\Phi^2\delta_{|r_1-r_2|,1}\mathcal{G}_{rr_1}(t,t_1)\mathcal{G}_{r_2 0}(t_1,0) \\ D_{\mathrm{C}}(t) &= -\mathrm{i}\sum_{r=\pm 1}\sum_{r_1 r_2}\int_0^{t_1}\mathrm{d}t_1\,\Phi\mathcal{J}_0'(r_1,r_2,t_1) \\ &\quad\times\ \mathcal{G}_{rr_1}(t,t_1)\mathcal{G}_{r_2 0}(t_1,0) \end{aligned} \tag{20}$$

where $\mathcal{G}_{r_1 r_2}(t_1,t_2) = \langle r_1|\mathcal{G}(t_1,t_2)|r_2\rangle$.

Although (20) provides a general definition of $D(t)$, its numerical evaluation represents a hard task mainly due to the complex nature of the relaxation operator. However, in the non-adiabatic limit, $\mathcal{J}(t)$ can be expressed in an improved way, making the calculation of $D(t)$ easier.

3.3. Diffusion coefficient: approximated expression

The time derivative of $\mathcal{J}(t)$ measures the system memory at time t of a vibron–phonon interaction occurring at time $t = 0$. As detailed in [2, 3], the creation of a vibron on a site $x = 0$ yields a contraction of the H bonds surrounding the excited site. The memory of this interaction involves two contributions. First, the lattice memory at time t and on site x of the initial deformation is measured by the correlation function $C_{0x}(t)$. Then, the free propagation of the vibron from the excited site involves the product between an advanced and a retarded free propagator. For a fixed x value, $C_{0x}(t)$ behaves as a bell-shaped peak centered around the phonon propagation time $t_x = 2|x|/\Omega_{\mathrm{c}}$ and whose width is about the phonon correlation time $\tau_{\mathrm{c}} = 2/\Omega_{\mathrm{c}}$ (see section 4). In a lattice of H-bonded peptide units, the phonons propagate faster than the vibron and τ_{c} is very short when compared with the time required for a vibron to move. Consequently, the main contribution of the relaxation operator (13) involves terms in which an advanced vibron propagator exactly compensates the associated retarded propagator. As a consequence, our numerical study has revealed that $\mathcal{J}_0(t)$ is mainly diagonal and it reduces to

$$\mathcal{J}_0(r,\bar{r},t) \approx \delta_{r\bar{r}}(\Gamma_0(t) - \Gamma_r(t)) \tag{21}$$

where $\Gamma_r(t)$ is defined as

$$\Gamma_r(t) = 2\,\mathrm{Re}\sum_h \int_0^t \mathrm{d}t_1\, C_{0h}(t_1)|G_{0,r-h}(t_1)|^2. \tag{22}$$

In other words, $\mathcal{J}_0(t)$ only depends on the parameter $\Gamma_r^*(t) = \Gamma_0(t) - \Gamma_r(t)$ which defines the TCL expression of the so-called pure dephasing constant.

Indeed, due to dipole–dipole coupling, the vibron delocalizes along the lattice. Its eigenstates correspond to extended states written as a superimposition of local states $|x\rangle$. Therefore, $\Gamma_r^*(t)$ describes the decay of the coherence between two states $|x_1\rangle$ and $|x_2 = x_1 + r\rangle$ mediated by the phonons. This decay results from the random fluctuations of the energy difference $\Delta H_{x_2x_2}(t) - \Delta H_{x_1x_1}(t)$. According to the stochastic theory of dephasing (see, for instance, [37]), $\dot{\Gamma}_r^*(t)$ is defined in terms of the correlation function of this energy difference, i.e. $\dot{\Gamma}_r^*(t) = 2\,\mathrm{Re}(C_{00}(t) - C_{0r}(t))$ in a lattice with translational invariance. It thus involves the difference between the autocorrelation function of each site energy and the cross-correlation function between the two site energies. Nevertheless, as shown in (22), the stochastic approach must be generalized to account for the ability of the vibron to propagate. The correlation functions between site energies are thus modulated by the vibron propagator. Consequently, $\dot{\Gamma}_0(t)$ and $\dot{\Gamma}_r(t)$ generalize the concept of autocorrelation function and cross-correlation function between site energies, respectively.

The diagonal nature of $\mathcal{J}_0(t)$ provides an improved expression of $D(t)$. Indeed, the unperturbed evolution operator $\mathcal{U}_0(t)$ is also diagonal and its matrix elements are written as $\mathcal{U}_0(r,\bar{r},t) \approx \delta_{r\bar{r}}\exp(-\phi_r(t))$. The function $\phi_r(t)$ is the time integral of the dephasing constant as

$$\phi_r(t) = \int_0^t \mathrm{d}t_1\,\Gamma_r^*(t_1). \tag{23}$$

Consequently, the knowledge of $\mathcal{U}_0(t)$ yields $\mathcal{G}(t)$ so that the two contributions of the diffusion coefficient (20) are finally

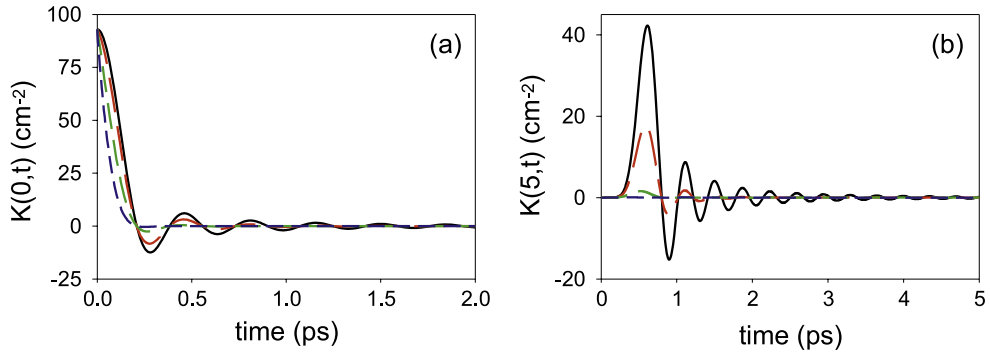

Figure 1. Time evolution of $K(x,t)$ at $T = 310$ K for (a) $x = 0$ and (b) $x = 5$ and for $\delta = 0$ nN Å^{-2} (full line), $\delta = 5$ nN Å^{-2} (long dashed line), $\delta = 10$ nN Å^{-2} (medium dashed line) and $\delta = 15$ nN Å^{-2} (short dashed line).

written as

$$D_{\mathrm{B}}(t) = 2\Phi^2 \mathrm{e}^{-\phi_1(t)} \int_0^t \mathrm{d}t_1\, \mathrm{e}^{\phi_1(t_1)}$$
$$D_{\mathrm{C}}(t) = 2\Phi^2 \mathrm{e}^{-\phi_1(t)} \int_0^t \mathrm{d}t_1\, \mathrm{e}^{\phi_1(t_1)} \eta(t_1) \qquad (24)$$

where $\eta(t)$, defined in terms of $\mathcal{J}_0'(t)$, is expressed as

$$\eta(t) = \frac{2}{\Phi}\,\mathrm{Im} \int_0^t \mathrm{d}t_1 \sum_h C_{0h}(t_1) G_{0,h}(t_1) G^*_{0,h+1}(t_1). \qquad (25)$$

Equation (24) is the main result of the present study. It provides a rather simple definition of the diffusion coefficient whose time evolution gives key information about the way the vibron–phonon interaction modifies the quantum propagation of the vibron. Note that the evaluation of (24) needs the knowledge of $C_{x_1x_2}(t)$ whose expression is given in the appendix.

4. Numerical results

In this section, the previous formalism is applied to evaluate the time-dependent diffusion coefficient that characterizes the motion of a vibron along a lattice of H-bonded peptide units. To proceed, typical values for the parameters are used: $\omega_0 = 1660$ cm^{-1}, $\Phi = 7.8$ cm^{-1}, $W = 15$ N m^{-1} and $M = 1.8 \times 10^{-25}$ kg. The vibron–phonon coupling strength is fixed to $\chi = -8$ pN whereas the cubic anharmonicity δ is considered as a free parameter. In that case, one obtains $\Omega_{\mathrm{c}} = 96.86$ cm^{-1}, $\tau_{\mathrm{c}} = 0.11$ ps and $E_{\mathrm{B}} = 0.21$ cm^{-1} so that the non-adiabatic weak coupling limit is reached.

At biological temperatures ($T = 310$ K), the time evolution of $K(x,t) = \mathrm{Re}\, C_{0x}(t)$ is illustrated in figure 1. For harmonic phonons, $K(0,t)$ behaves as a peak centered on $t = 0$ and whose amplitude is 92.94 cm^{-2} (figure 1(a)). It rapidly decays over a timescale of about 0.12 ps (i.e. about τ_{c}) by exhibiting damped oscillations. For $x \neq 0$, $K(x,t)$ is equal to zero until the time reaches the phonon propagation time $t_x = x\tau_{\mathrm{c}}$. At that time, $K(x,t)$ shows a peak whose amplitude is about $K(0,0)/2$ and whose width is about $2\tau_{\mathrm{c}}$. Then, $K(x,t)$ tends to zero by still exhibiting small amplitude damped oscillations (figure 1(b)). When δ is turned on, a different behavior takes place. As δ increases, the width of $K(0,t)$ decreases whereas its amplitude is not modified. For instance, the width varies between 0.11 ps for $\delta = 5$ nN Å^{-2} and 0.04 ps for $\delta = 15$ nN Å^{-2} (figure 1(a)). Moreover, the anharmonicity prevents the occurrence of damped oscillations so that $K(0,t)$ rapidly vanishes. For $x \neq 0$, the main peak of $K(x,t)$ takes place for a time slightly smaller than t_x. Although the anharmonicity does not significantly affect the width of the peak, it is responsible for a strong decay of its amplitude. This amplitude is equal to 17.71 and 0.05 cm^{-2} for $\delta = 5$ and 15 nN Å^{-2}, respectively (figure 1(b)).

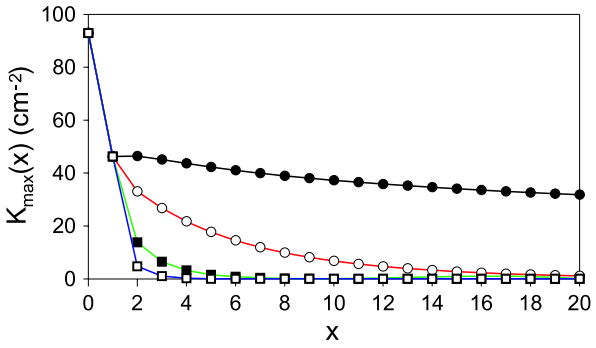

Figure 2. $K_{\max}(x)$ versus x at $T = 310$ K and for $\delta = 0$ nN Å^{-2} (full circles), $\delta = 5$ nN Å^{-2} (open circles), $\delta = 10$ nN Å^{-2} (full squares) and $\delta = 15$ nN Å^{-2} (open squares).

The influence of the phonon anharmonicity on the maximum value $K_{\max}(x)$ of $K(x,t)$ is displayed in figure 2. When $\delta = 0$, $K_{\max}(x)$ shows a slowly varying algebraic decay provided that $x > 0$. In the same time, we have verified that the damped oscillations which occur after the main peak take place over a timescale which increases with x. This feature counterbalances the algebraic decay of the peak amplitude so that the time integral of each correlation function is finally x-independent. For anharmonic phonons, the peak amplitude exhibits an exponential decay. The correlations take place over a finite length scale defined as the correlation length ξ which ranges between 5.06 and 0.65 when δ varies between 5 and 15 nN Å^{-2}. Note that the localized nature of the correlation functions induces an exponential decay of the corresponding integrated correlations.

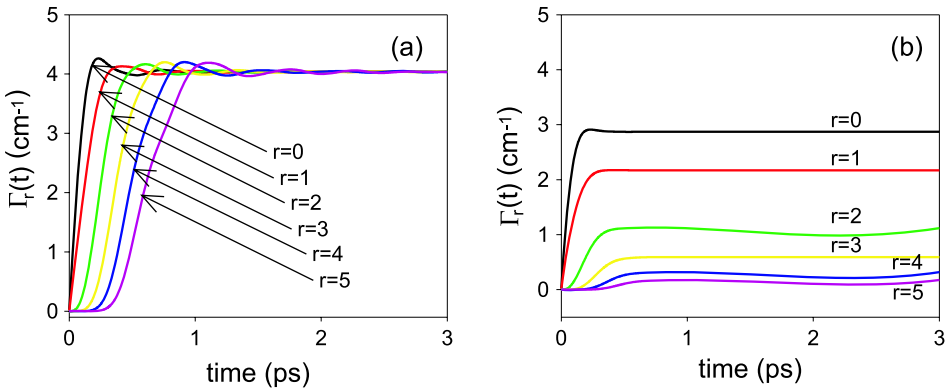

Figure 3. Time evolution of $\Gamma_r(t)$ at $T = 310$ and for (a) $\delta = 0$ nN Å^{-2} and (b) $\delta = 10$ nN Å^{-2}.

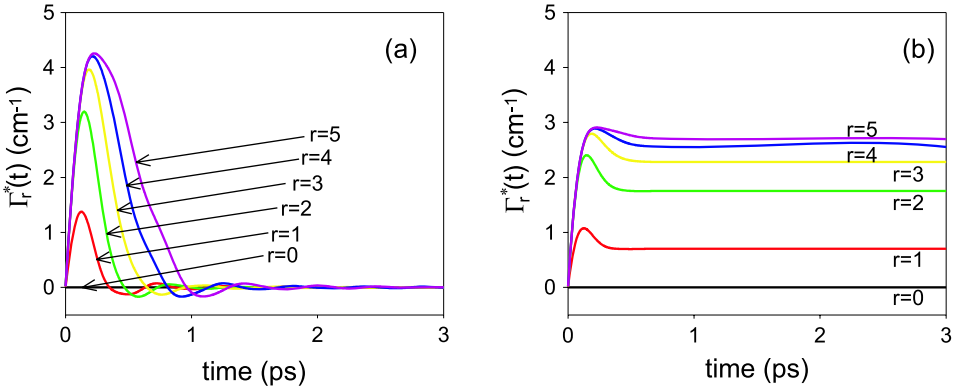

Figure 4. Time evolution of $\Gamma_r^*(t)$ at $T = 310$ K and for (a) $\delta = 0$ nN Å^{-2} and (b) $\delta = 10$ nN Å^{-2}.

The time evolution of $\Gamma_r(t)$ at $T = 310$ K is shown in figure 3. When $\delta = 0$ (figure 3(a)), $\Gamma_r(t)$ is initially equal to zero over a timescale which increases with r. Then, it rapidly increases to finally show small-amplitude damped oscillations around an r-independent value $\Gamma_r(\infty) \approx 4.03$ cm^{-1}. The time for which $\Gamma_r(t)$ reaches $\Gamma_r(\infty)/2$ scales as $0.11r$ ps indicating that phonons with sound velocity carry correlations between site energies. These results are qualitatively temperature-independent. Nevertheless, from a quantitative point of view, $\Gamma_r(\infty)$ increases linearly with temperature over the range 100–310 K. For anharmonic phonons (figure 3(b)), a different behavior takes place and three main features emerge. First, $\Gamma_r(t)$ reaches a permanent regime after a timescale slightly shorter than t_r. Then, the anharmonicity prevents the occurrence of damped oscillations. Finally, in the permanent regime, $\Gamma_r(\infty)$ exhibits a strong r dependence. For small δ values, $\Gamma_r(\infty)$ decreases almost linearly with r whereas an exponential decay occurs for larger δ values. For $\delta = 5$ nN Å^{-2}, $\Gamma_r(\infty)$ is equal to 3.70 and 1.71 cm^{-1} for $r = 0$ and 5, respectively, whereas for $\delta = 10$ nN Å^{-2}, it varies between 2.87 cm^{-1} for $r = 0$ and 0.17 cm^{-1} for $r = 5$.

In figure 4, the time evolution of the dephasing constant $\Gamma_r^*(t)$ is shown at $T = 310$ K. For harmonic phonons (figure 4(a)), the time dependence of $\Gamma_r^*(t)$ is qualitatively independent on both r and T. Note that $\Gamma_{r=0}^*(t) = 0$ since incoherent hops are forbidden. Initially equal to zero, $\Gamma_r^*(t)$ rapidly increases to reach a maximum value which indicates that dephasing takes place in the short time limit. Then, $\Gamma_r^*(t)$ decreases so that a rephasing mechanism occurs. It finally converges to zero by exhibiting small-amplitude damped oscillations. From $t = 0$, $\Gamma_r^*(t)$ reaches half of its maximum value at $t = 0.054$ ps (i.e. about $\tau_c/2$) $\forall r$. By contrast, the maximum value of $\Gamma_r^*(t)$ increases with r. Similarly, during its decay, the time for which $\Gamma_r^*(t)$ reaches half of its maximum value increases with r. It scales as $0.10r$ ps, revealing that phonon propagation is at the origin of this dephasing–rephasing process. Consequently, the coherence between two states $|x\rangle$ and $|x + r\rangle$ is finally restored after a timescale of about t_r. When δ is turned on (figure 4(b)), $\Gamma_{r=0}^*(t)$ still vanishes. Therefore, for $r > 0$, $\Gamma_r^*(t)$ rapidly increases in the short time limit. It reaches a maximum value whose amplitude increases with r but decreases with δ. As previously, in the short time limit, $\Gamma_r^*(t)$ reaches half of its maximum value after a time almost r-independent. Then, $\Gamma_r^*(t)$ decreases to finally converge to a non-vanishing constant value $\Gamma_r^*(\infty)$. The permanent regime is reached after a time which still increases linearly with r. Note that the damped oscillations tend to disappear when δ is turned on. These features show that the anharmonicity prevents the occurrence of a complete rephasing so that the coherence between two states $|x\rangle$ and $|x + r\rangle$ finally decays according to the rate $\Gamma_r^*(\infty)$.

In figure 5, special attention is paid to characterize the key parameters $\Gamma_1^*(t)$ and $\eta(t)$ which enter the definition of

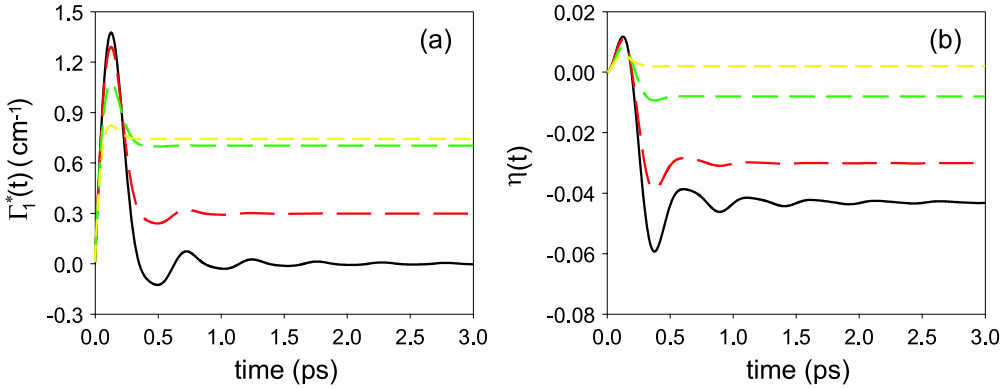

Figure 5. Time evolution of (a) $\Gamma_1^*(t)$ and (b) $\eta(t)$ for $T = 310$ K and for $\delta = 0$ nN Å^{-2} (full line), $\delta = 5$ nN Å^{-2} (long dashed line), $\delta = 10$ nN Å^{-2} (medium dashed line) and $\delta = 15$ nN Å^{-2} (short dashed line).

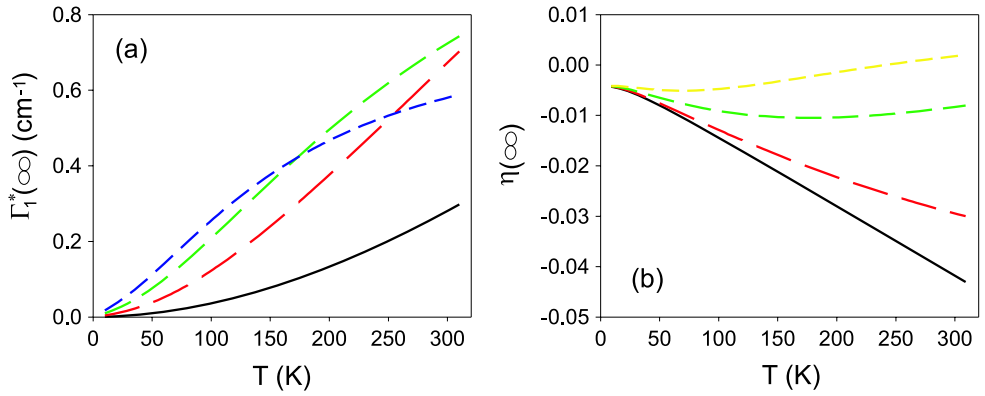

Figure 6. (a) $\Gamma_1^*(\infty)$ versus T for $\delta = 5$ nN Å^{-2} (full line), $\delta = 10$ nN Å^{-2} (long dashed line), $\delta = 15$ nN Å^{-2} (medium dashed line) and $\delta = 20$ nN Å^{-2} (short dashed line). (b) $\eta(\infty)$ versus T for $\delta = 0$ nN Å^{-2} (full line), $\delta = 5$ nN Å^{-2} (long dashed line), $\delta = 10$ nN Å^{-2} (medium dashed line) and $\delta = 15$ nN Å^{-2} (short dashed line).

the diffusion coefficient. As shown in figure 5(a), $\Gamma_1^*(t)$ first increases to reach a maximum value whose amplitude decreases with δ from 1.37 cm^{-1} for $\delta = 0$ to 0.82 cm^{-1} for $\delta = 15$ nN Å^{-2}. This maximum takes place for a time of about 0.12 ps $\forall\,\delta$. Then $\Gamma_1^*(t)$ decreases to finally converge to a constant value $\Gamma_1^*(\infty)$. For the parameters used in figure 5(a), $\Gamma_1^*(\infty)$ increases with δ and it is successively equal to 0, 0.3, 0.70 and 0.74 cm^{-1} for $\delta = 0$, 5, 10 and 15 nN Å^{-2}. However, for larger δ values, we have observed that $\Gamma_1^*(\infty)$ tends to decay with δ (not drawn in figure 5(a)). For harmonic phonons, $\eta(t)$ rapidly increases from zero to reach a maximum value after typically 0.12 ps (figure 5(b)). Then, it decreases to finally converge to $\eta(\infty) \approx -0.043$ by exhibiting damped oscillations. When δ is turned on, $\eta(t)$ basically behaves as previously. Nevertheless, the oscillations tend to disappear and the permanent value $\eta(\infty)$ increases with δ. Still negative for small δ values ($\eta(\infty) = -3 \times 10^{-2}$ for $\delta = 5$ nN Å^{-2}), it becomes positive for large δ values ($\eta(\infty) = 2 \times 10^{-3}$ for $\delta = 15$ nN Å^{-2}).

The temperature dependence of $\Gamma_1^*(\infty)$ is illustrated in figure 6(a). The dephasing constant tends to zero as the temperature vanishes and it increases with T over the range 0–310 K. Nevertheless, its behavior depends on both T and δ. Over the range 0–100 K, $\Gamma_1^*(\infty)$ typically scales as T^β. The exponent β is greater than unity whatever the δ values considered in figure 6(a). It tends to 2 in the weak anharmonicity limit and it reaches 1.84 and 1.20 when $\delta = 5$ and $\delta = 10$ nN Å^{-2}, respectively. Over the range 200–310 K, $\Gamma_1^*(\infty)$ still behaves as T^β. However, two regimes occurs depending on the δ values. For small δ values, β is still greater than unity and it reduces to 1.83 and 1.41 for $\delta = 5$ and 10 nN Å^{-2}, respectively. By contrast, for larger δ values, β becomes smaller than unity, indicating a slowdown in the increase of the dephasing constant with temperature. For instance, β reduces to 0.52 for $\delta = 20$ nN Å^{-2}.

Figure 6(b) displays the temperature dependence of the parameter $\eta(\infty)$. At very low temperatures, $\eta(\infty) = -4.2 \times 10^{-3}$ is independent of δ. By contrast, at higher temperatures, two regimes occur. For harmonic phonons, $\eta(\infty)$ decreases linearly with T. By contrast, when δ is turned on, a slowdown in its decrease is observed for $\delta = 5$ nN Å^{-2}. For larger δ values, $\eta(\infty)$ decreases with T until it reaches a minimum value to finally increase with T. This behavior is enhanced by the anharmonicity and $\eta(\infty)$ becomes positive for $\delta = 15$ nN Å^{-2} at $T = 310$ K.

The time evolution of both the band diffusion coefficient and the cross-diffusion coefficient is illustrated in figure 7.

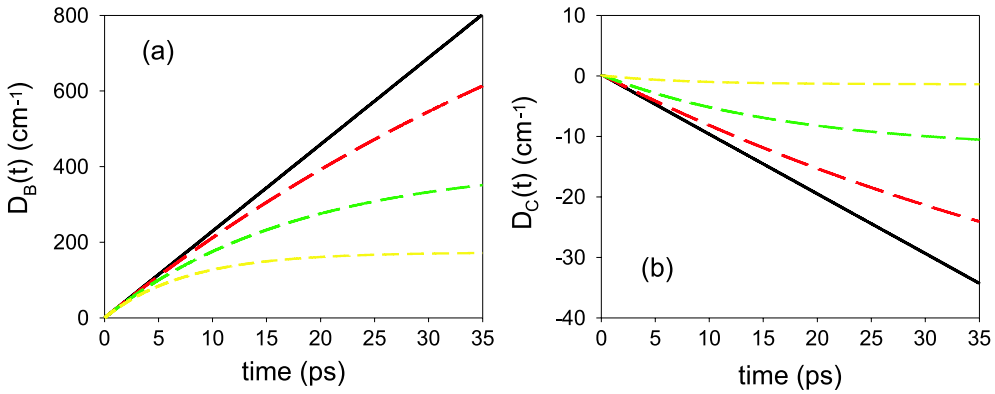

Figure 7. Time evolution of (a) $D_B(t)$ and (b) $D_C(t)$ for $T = 310$ K and for $\delta = 0$ nN Å^{-2} (full line), $\delta = 2.5$ nN Å^{-2} (long dashed line), $\delta = 5$ nN Å^{-2} (medium dashed line) and $\delta = 10$ nN Å^{-2} (short dashed line).

For harmonic phonons, $D_B(t)$ increases linearly with respect to time. Such a behavior is temperature-independent and it occurs even in the short time limit. In fact, the numerical calculations reveal that $D_B(t) \approx 2\Phi^2 t$. By contrast, $D_C(t)$ almost vanishes over a timescale of about 0.25 ps, i.e. about $2\tau_c$ (not distinguishable in figure 7). Then, it becomes negative and it decreases linearly with time. The higher the temperature is, the faster is its decay. Nevertheless, figure 7 shows that $D_C(t)$ represents a very small correction when compared with $D_B(t)$. Consequently, after a timescale of about $2\tau_c$, $D(t)$ is proportional to time, indicating that the vibron propagates coherently along the lattice in spite of its coupling with the phonon bath. At biological temperatures, this wavelike behavior results from a coherent motion according to an effective hopping constant $\hat{\Phi} = 7.6$ cm^{-1}, i.e. slightly smaller than the bare hopping constant $\Phi = 7.8$ cm^{-1}. Note that the T dependence of $D_C(t)$ shows that $\hat{\Phi}$ is a slowly decaying function of the temperature.

For anharmonic phonons, the behavior of the diffusion coefficients strongly depends on δ over the timescale considered in figure 7. Indeed, for $\delta = 2.5$ nN Å^{-2}, $D_B(t)$ still increases with time but according to a law which increases slower than the linear law observed in the harmonic situation. Such a behavior has been fitted by the following power law: $D_B(t) \propto t^{0.85}$. In the same way, after about $2\tau_c$, $D_C(t)$ decreases with time and its behavior is well represented by the power law $D_C(t) \propto -t^{0.87}$. The similarity between the two exponents shows that both $D_B(t)$ and $D_C(t)$ are governed by the same physics so that $D(t)$ scales as t^{λ}, with $\lambda \approx 0.86 \pm 1$. In other words, the motion of the vibron is neither coherent nor incoherent but a mixing between the two regimes takes place over the timescale represented in figure 7. For larger δ values, the slowdown of both the increase of $D_B(t)$ and the decrease of $D_C(t)$ is enhanced. Therefore, for $\delta = 10$ nN Å^{-2}, the two diffusion coefficients converge to a constant value in the long time limit, i.e. typically for $t > 10$ ps. The band diffusion coefficient tends to $D_B(\infty) = 171.48$ cm^{-1} whereas $D_C(\infty) = -1.37$ cm^{-1}. An incoherent regime occurs and the vibron diffuses along the lattice according to the diffusion coefficient $D(\infty) = 170.11$ cm^{-1}. When $\delta = 15$ nN Å^{-2} a similar behavior occurs although $D_C(\infty)$ now tends to a positive value equal to 0.32 cm^{-1}. However, this value is negligible when compared with $D_B(\infty) = 166.66$ cm^{-1} which still dominates the full diffusion coefficient (not drawn in figure 7).

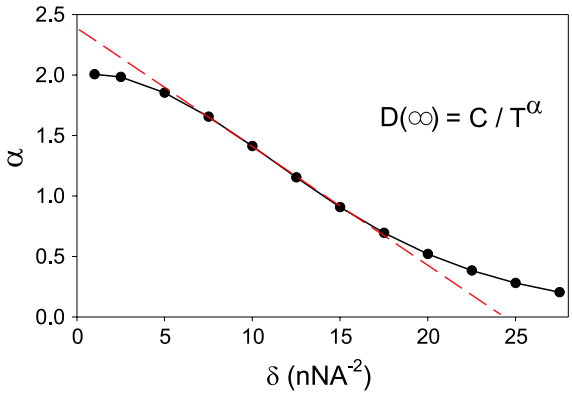

Figure 8. α versus δ on the temperature range 200–310 K.

Long time simulations have been carried out to extract the temperature dependence of the incoherent diffusion coefficient $D(\infty)$ in the high temperature limit, i.e. over the range 200–310 K. In a general way, $D(\infty)$ decreases with T and its behavior is well represented by a power law $D(\infty) = C/T^{\alpha}$. As shown in figure 8, the value of the exponent α strongly depends on δ and three different regimes occur. In the weak anharmonicity limit, i.e. when $\delta < 5$ nN Å^{-2}, α is typically about 2 so that $D(\infty)$ rapidly decreases with temperature according to the power law $D(\infty) \propto 1/T^2$. In the intermediate regime, i.e. when $\delta \in [5, 15]$ nN Å^{-2}, the exponent α decreases almost linearly with δ. It ranges between 1 and 2 indicating a slowdown in the decay of $D(\infty)$ with the temperature. Note that $D(\infty) \propto 1/T$ when $\delta = 13.82$ nN Å^{-2}. This feature is enhanced in the strong anharmonicity limit, i.e. $\delta > 15$ nN Å^{-2}, where α becomes smaller than unity. The long time diffusion coefficient is thus a slowly decaying function of the temperature which becomes almost temperature-independent in the very strong anharmonicity limit ($\alpha = 0.20$ for $\delta = 27.5$ nN Å^{-2}).

To conclude this section, let us evaluate the relevant parameters for a spine of H-bonded peptide units involved in an α-helix. To proceed, the H bond is modeled with a Lennard-Jones potential [40] so that W and δ satisfy $\delta(\text{nN Å}^{-2}) = 2.1W(\text{N m}^{-1})/r_0(\text{Å})$. The equilibrium distance of the O$\cdots$H bond being about $r_0 = 1.92$ Å [1], one obtains $\delta = 16.40$ nN Å^{-2}. At $T = 310$ K, the phonon decay rate is $\gamma = 82.55$ cm^{-1} and the dephasing constant reaches $\Gamma_1^*(\infty) = 0.70$ cm^{-1}. The dephasing time is equal to $T_2 = 7.5$ ps and the diffusion coefficient is $D(\infty) = 172.54$ cm^{-1}, i.e. about 9.48×10^{-2} cm^2 s^{-1} with a lattice parameter equal to 5.4 Å. In the high temperature limit, $D(\infty)$ typically scales as $1/T^{0.78}$.

5. Discussion

The numerical results have revealed that the vibronic transport strongly depends on the nature of the phonons. For harmonic phonons, it has been shown that the vibron–phonon interaction yields a dephasing–rephasing mechanism in the short time limit which prevents the occurrence of the vibron diffusivity. The vibron propagates freely along the lattice as if it was insensitive to the bath. Keeping its wavelike nature, it induces a coherent vibrational energy flow characterized by a diffusion coefficient which increases linearly with time. By contrast, when the anharmonicity is turned on, the rephasing process no longer compensates the dephasing mechanism. After a transient regime, the bath tends to destroy the coherent behavior of the vibron. Dephasing-limited band motion takes place, resulting in a transition between a coherent motion in the short time limit and an incoherent motion in the long time limit. The vibrational energy flow is finally mediated according to an incoherent diffusion mechanism. The corresponding diffusion coefficient typically scales as $1/T^2$ in the weak anharmonicity limit whereas it becomes a slowly decaying function of temperature in the strong anharmonicity limit.

As shown in section 3, the influence of the phonons on the vibron dynamics is defined in terms of the vibron–phonon coupling correlation function. Depending on whether the phonons are harmonic or not, this function behaves differently resulting in a vibron dynamics either coherent or incoherent. To understand this feature, special attention is first paid to characterize $C_{x_1x_2}(t)$ by using the so-called Debye model.

5.1. Vibron–phonon coupling correlation function

Within the Debye model, the phonon dispersion curve is linearized so that $\Omega_q \approx c|q|$, where $c = \Omega_c/2$ is the sound velocity. Therefore, by inserting this expression into (A.6) at high temperature, one obtains

$$K(x,t) = E_B k_B T e^{-\gamma t}[f(x-ct) + f(x+ct)]$$
$$S(x,t) = -(2k_BT)^{-1}\dot{K}(x,t) \tag{26}$$

where $f(z)$, defined in terms of sine cardinal functions, can be approximated by the rectangular function $f(z) = 1$ for $z \in [-1, 1]$ and zero otherwise. Therefore, $K(x,t)$ reduces to

$$K(x,t) = \begin{cases} (1+\delta_{x0})E_B k_B T e^{-\gamma t} & \text{if } t \in [t_{x-1}, t_{x+1}] \\ 0 & \text{otherwise} \end{cases} \tag{27}$$

where $t_x = x\tau_c$ is the phonon propagation time.

Equation (27) captures the main part of the physics involved in the correlation function at biological temperatures. Indeed, for $x = 0$, it defines a peak centered on $t = 0$ and whose amplitude is equal to $2E_Bk_BT$. For the parameters used in the simulation, this amplitude, equal to 92.55 cm^{-2}, is almost equal to the numerical value (figure 1). The width of this peak is equal to τ_c for harmonic phonons whereas it reduces to $1/\gamma$ when δ is turned on. Since γ scales as δ^2 (see (A.4)), the width decreases with δ as observed in figure 1. For non-vanishing x values and for $\delta = 0$, the peak amplitude is E_Bk_BT and its width is equal to $2\tau_c$. Note that (27) describes neither the algebraic decay of the peak amplitude nor the occurrence of damped oscillations since both features originate from the dispersive nature of the phonons which has been neglected within the Debye model. Nevertheless, the Debye model yields integrated correlations in rather good agreement with the numerical calculations. For anharmonic phonons (27) shows that the peak amplitude decreases with the distance according to the exponential law $K_{\max}(x) = E_Bk_BT\exp(-x/\xi)$, where $\xi = \Omega_c/2\gamma$ defines the correlation length ($x > 0$). At biological temperatures, ξ varies between 6.31 and 0.65 when δ ranges between 5 and 15 nN Å^{-2}, in relatively good agreement with the numerical values (figure 2).

In other words, for independent phonons, the bath exhibits spatial correlations over an infinite length scale. By contrast, the phonon–phonon interaction induces a finite lifetime $T_1 \approx 1/\gamma$ for each phonon mode. As a result, spatial correlations occur over a length scale $\xi = cT_1$ defined as the distance covered by the phonons during their lifetime.

5.2. Integrated correlation functions

To understand the way spatial correlations in the bath affect the vibron dynamics, let us evaluate the integrated correlation functions $\Gamma_r(t)$. Within the non-adiabatic limit, the main contribution of $\Gamma_r(t)$ involves the term that characterizes a coincidence between the vibron propagator and the coupling correlation function. Therefore, from (22), $\Gamma_r(t)$ reduces to

$$\Gamma_r(t) \approx 2\int_0^t \mathrm{d}t_1\, K(r,t_1). \tag{28}$$

Equation (28) reveals that $\dot{\Gamma}_r(t)$ is two times the real part of the correlation function between two site energies separated by the distance r. It measures the lattice memory at time t and on site r of an initial H-bond contraction induced by the vibron–phonon interaction on site $r = 0$. Therefore, for $r = 0$, inserting (27) into (28) for harmonic phonons yields $\Gamma_0(t)$ in terms of $\Gamma = 8E_Bk_BT/\Omega_c$ (see section 2.2) as

$$\Gamma_0(t) \approx \Gamma\begin{cases} t/\tau_c & \text{if } t \leqslant \tau_c \\ 1 & \text{if } t > \tau_c. \end{cases} \tag{29}$$

For $r > 0$, $\Gamma_r(t)$ vanishes for $t < t_{r-1}$ and it satisfies

$$\Gamma_r(t) \approx \Gamma \begin{cases} [t/\tau_c - (r-1)]/2 & \text{if } t \in [t_{r-1}, t_{r+1}] \\ 1 & \text{if } t > t_{r+1}. \end{cases} \tag{30}$$

For $r = 0$, the lattice memory of the initial interaction takes a significant value at time $t = 0$. Then it vanishes for $t > \tau_c$, indicating that the phonons have left the excited region. Consequently, $\Gamma_0(t)$ first increases to finally converge to a constant value $\Gamma_0(\infty) = \Gamma$ (see figure 3). At biological temperatures, one obtains $\Gamma = 3.82$ cm^{-1}. The small discrepancy with the numerical value equal to 4.03 cm^{-1} originates from the validity of the non-adiabatic limit. It tends to disappear when Φ/Ω_c is reduced. For $r \neq 0$, no memory occurs until time reaches t_{r-1} which represents the time needs for the phonons to cover $r-1$ sites. Then, the correlation switches on, provided that $t \in [t_{r-1}, t_{r+1}]$, i.e. when the phonons are located around the site r. Finally, the memory vanishes for $t > t_{r+1}$, indicating that the phonons propagate far from the site r. Consequently, $\Gamma_r(t)$ turns on when $t > t_{r-1}$ to finally converge to a constant value $\Gamma_r(\infty) = \Gamma$ when $t > t_{r+1}$. Since the bath exhibits spatial correlations over an infinite length scale, $\Gamma_r(\infty)$ is r-independent as observed in figure 3.

When $\delta \neq 0$, by inserting (27) into (28) for $r = 0$, one obtains

$$\Gamma_0(t) \approx \frac{\Gamma}{\gamma\tau_c} \begin{cases} 1 - e^{-\gamma t} & \text{if } t \leqslant \tau_c \\ 1 - e^{-\gamma\tau_c} & \text{if } t > \tau_c. \end{cases} \tag{31}$$

Similarly for $r > 0$, $\Gamma_r(t)$ vanishes for $t < t_{r-1}$ and it is defined as

$$\Gamma_r(t) \approx \frac{\Gamma}{2\gamma\tau_c} \begin{cases} e^{-\gamma t_{r-1}} - e^{-\gamma t} & \text{if } t \in [t_{r-1}, t_{r+1}] \\ e^{-\gamma t_{r-1}} - e^{-\gamma t_{r+1}} & \text{if } t > t_{r+1}. \end{cases} \tag{32}$$

For anharmonic phonons, the physics that defines the lattice memory is the same as the physics involved in the harmonic situation. However, the γ dependence of $\Gamma_r(t)$ results from the competition between the ability of the phonons to propagate and their finite lifetime. Indeed, for $r = 0$, (31) leads to $\dot{\Gamma}_0(t) = 4E_B k_B T \exp(-\gamma t)$ for $t < \tau_c$. This expression indicates that the lattice memory of the initial vibron–phonon coupling is modulated by the probability to observe the excited phonons before their annihilation due to phonon–phonon interactions. Consequently, the lattice memory decays with time in an exponential way. It finally vanishes when the phonons have left the excited site, i.e. when $t > \tau_c$. Therefore $\Gamma_0(t)$ converges to a constant value whose amplitude decreases with γ. For $r > 0$, the behavior of $\Gamma_r(t)$ originates from the r dependence of the probability that phonons cover $(r-1)$ sites before being annihilated. Since spatial correlations now occur over a finite length scale, the larger the distance r is, the smaller is the probability. As a result, $\Gamma_r(t)$ switches on when $t > t_{r-1}$. It converges to a constant value $\Gamma_r(\infty)$ which decays with distance according to an exponential law $\exp(-r/\xi)$. For instance, for $\delta = 5$ nN Å^{-2}, $\Gamma_r(\infty)$ is equal to 3.53 and 1.74 cm^{-1} for $r = 0$ and 5, respectively, whereas for $\delta = 10$ nN Å^{-2}, it varies between 2.83 cm^{-1} for $r = 0$ and 0.17 cm^{-1} for $r = 5$, in close agreement with the numerical results.

The knowledge of $\Gamma_r(t)$ yields analytical expressions for $\Gamma_r^*(t)$. We have verified that the Debye model provides results in rather good agreement with our numerical observations (figures 4 and 5). Nevertheless, to simplify the discussion, special attention will be paid to study $\Gamma_1^*(t)$ only, since it enters the definition of the diffusion coefficient. We thus successively consider the harmonic and anharmonic situations.

5.3. Transport properties for a vibron coupled with harmonic phonons

The dephasing constant $\Gamma_1^*(t)$ describes the influence of the bath on the coherence between neighboring vibron local states. Within the non-adiabatic limit, it reduces to

$$\Gamma_1^*(t) \approx 2\int_0^t dt_1\,[K(0,t_1) - K(1,t_1)]. \tag{33}$$

We thus recover the standard definition of the dephasing constant whose time derivative is the real part of the correlation function of the energy difference $\Delta H_{xx}(t) - \Delta H_{x\pm1x\pm1}(t)$. It thus involves the difference between the autocorrelation function of each site energy (i.e. $\dot{\Gamma}_0(t)$) and the cross-correlation function between the two neighboring site energies (i.e. $\dot{\Gamma}_1(t)$).

For harmonic phonons, by using (29) and (30), one obtains

$$\Gamma_1^*(t) \approx \frac{\Gamma}{2\tau_c} \begin{cases} t & \text{if } 0 < t < \tau_c \\ 2\tau_c - t & \text{if } \tau_c < t < 2\tau_c \\ 0 & \text{if } t > 2\tau_c. \end{cases} \tag{34}$$

The time evolution of $\Gamma_1^*(t)$ can be interpreted as follows. Initially on a site x, the vibron interacts with the phonons. A lattice deformation occurs and it induces a local variation of the vibron energy. It yields random fluctuations of the phase difference between the weight of the states $|x\rangle$ and $|x \pm 1\rangle$ over which the vibron tends to delocalize. The fluctuations break the coherent nature of this superimposition, giving rise to a dephasing mechanism. This quantum decoherence is described by $\Gamma_1^*(t)$ which increases with time provided that $t < \tau_c$. However, when $t \geqslant \tau_c$, the initial deformation reaches the sites $x \pm 1$. Consequently, correlations between neighboring sites switch on so that the phase relation between the local states involved in the superimposition is restored. The coherent nature of the superimposition recurs, resulting in the occurrence of the rephasing mechanism. The corresponding dephasing constant thus decreases with time. Finally, for $t > 2\tau_c$, the lattice deformation has left the excited region and $\Gamma_1^*(t)$ finally vanishes. This scenario, together with (34), provides a physical interpretation of the numerical observations displayed in figures 4 and 5.

The dephasing–rephasing mechanism yields a time-resolved picture of the influence of the vibron–phonon interaction in momentum space. Indeed, the vibron eigenstates refer to a Bloch wave with wavevector K and eigenfrequency ω_K (see section 2.1) so that dephasing in real space

characterizes lifetime in momentum space. Therefore, to second order with respect to ΔH, this lifetime originates from the scattering of a vibron with wavevector K into an eigenstate with wavevector $K \pm q$ via the exchange of a phonon with wavevector q. Such a process occurs if energy conservation takes place, i.e. if $\omega_{K\pm q} = \omega_K \pm \Omega_q$. However, in the non-adiabatic limit, i.e. provided that $4\Phi < \Omega_c$, the energy cannot be conserved so that the emission or the absorption of a phonon does not correspond to a real process. Consequently, the vibron is only able to exchange a virtual phonon which is first emitted and then immediately reabsorbed, and vice versa. The dephasing–rephasing mechanism is thus the counterpart in real space of the virtual phonon emission–absorption mechanism in momentum space.

The dressing of the vibron by virtual phonons induces a renormalization of the vibron hopping constant. This renormalization is described by the parameter $\eta(t)$ involved in the cross-diffusion coefficient (25). Within the non-adiabatic limit, $\eta(t)$ is expressed as

$$\eta(t) \approx 2\int_0^t \mathrm{d}t_1\, t_1[K(0,t_1) - K(1,t_1)]. \tag{35}$$

By using (29) and (30) for $\delta = 0$, one obtains

$$\eta(t) \approx \frac{\Gamma}{4\tau_c}\begin{cases} t^2 & \text{if } 0 < t < \tau_c \\ 2\tau_c^2 - t^2 & \text{if } \tau_c < t < 2\tau_c \\ -2\tau_c^2 & \text{if } t > 2\tau_c. \end{cases} \tag{36}$$

As observed in figure 5(b), $\eta(t)$ first increases with time to reach a maximum value. It then decreases to finally converge to a negative value $\eta(\infty) = -8E_B k_B T/\Omega_c^2$. Note that this value, equal to -0.039 at $T = 310$ K, is close to the numerical value -0.043.

In that context, after a time of about $2\tau_c$, the rephasing process exactly compensates the initial dephasing. The dephasing constant vanishes and $\eta(t)$ converges to a constant value $\eta(\infty)$. Therefore, (24) can be solved easily, leading to a diffusion coefficient written as

$$D(t) \approx 2\Phi^2(1 + \eta(\infty))t. \tag{37}$$

Since the dephasing–rephasing mechanism occurs over a timescale shorter than the time required for the vibron to move, it was as if the vibron was insensitive to the phonon bath. As a result, the vibron keeps its wavelike nature and a coherent energy transfer takes place along the lattice. The corresponding time-dependent diffusion coefficient increases linearly with time, as observed in figure 7, so that the vibron mean square displacement scales as t^2. This coherent motion is characterized by the effective hopping constant $\hat{\Phi} = \Phi\sqrt{1+\eta(\infty)}$ approximately given by

$$\hat{\Phi} \approx \Phi\left(1 - \frac{4E_B k_B T}{\Omega_c^2}\right). \tag{38}$$

Equation (38) shows that $\hat{\Phi}$ is the weak coupling limit of the effective hopping constant that arises in the small polaron approach at high temperature [2]. Equal to 7.64 cm^{-1} for $T = 310$ K, it is almost identical to the value extracted from figure 7.

Note that similar results have been obtained within the frame of the generalized Fulton–Gouterman transformation which diagonalizes the coupled exciton–phonon Hamiltonian and yields an exact expression for the mean square displacement [38, 39]. The authors showed that there is no excitonic diffusivity under the assumed translational invariance at zero temperature. Nevertheless, they claimed that, in most theories of exciton transport, the phonon subsystem is considered as a bath which causes the exciton propagation to become diffusive. Our results clarify this point and reveal that spatial correlations over an infinite length scale in the bath prevent the diffusive motion to occur, even at finite temperature. Nevertheless, this coherent regime emerges when the non-adiabatic weak coupling limit is reached and when the phonons describe independent excitations.

5.4. Transport properties for a vibron coupled with anharmonic phonons

When the anharmonicity is turned on, a different situation takes place. Indeed, by using (31) and (32), $\Gamma_1^*(t)$ is approximated as

$$\Gamma_1^*(t) \approx \frac{\Gamma}{2\gamma\tau_c}\begin{cases} 1 - \mathrm{e}^{-\gamma t} & \text{if } 0 < t < \tau_c \\ 1 - 2\mathrm{e}^{-\gamma\tau_c} + \mathrm{e}^{-\gamma t} & \text{if } \tau_c < t < 2\tau_c \\ (1 - \mathrm{e}^{-\gamma\tau_c})^2 & \text{if } t > 2\tau_c. \end{cases} \tag{39}$$

The physics that defines the time evolution of $\Gamma_1^*(t)$ is the same as the physics involved in the harmonic case. In the short time limit, a dephasing process takes place and the coherence between neighboring vibron local states decays. This decoherence originates from the random fluctuations of the site energies induced by the lattice deformation that emerges from the vibron–phonon interaction. The dephasing constant thus increases, provided that $t < \tau_c$. Then, a rephasing occurs since correlations between neighboring sites switch on due to the propagation of the lattice deformation. The dephasing constant thus decreases when time ranges between τ_c and $2\tau_c$. Finally, $\Gamma_1^*(t)$ becomes time-independent when $t > 2\tau_c$ since the phonons have left the excited region.

Nevertheless, the localized nature of the vibron–phonon coupling correlation function prevents the rephasing process to exactly compensate the dephasing process. The coherence between neighboring vibron states cannot be restored so that an irreversible quantum decoherence takes place. The dephasing constant no longer vanishes in the long time limit but it converges to a finite value defined as

$$\Gamma_1^*(\infty) = \frac{2E_B k_B T}{\gamma}(1 - \mathrm{e}^{-\gamma\tau_c})^2. \tag{40}$$

Equation (40) provides $\Gamma_1^*(\infty)$ values in a qualitatively good agreement with our numerical data. For instance, at $T = 310$ K, $\Gamma_1^*(\infty)$ is equal to 0.26, 0.66 and 0.77 cm^{-1} for $\delta = 5$, 10 and 15 nN Å^{-2}, respectively (see figure 5(a)). Moreover, it reveals that the origin of the temperature dependence of $\Gamma_1^*(\infty)$ is twofold. First, it results from the phonon population

which is proportional to $k_B T$ at biological temperatures. Then, it arises from the phonon decay rate γ which also increases linearly with T according to equation (A.4). At biological temperatures, both effects exactly compensate for each other so that the dephasing constant behaves as $\Gamma_1^*(\infty) \propto (1-e^{-T/T_0})^2$ with $k_B T_0 = 2W^3/\delta^2$. In the weak anharmonicity limit ($\gamma\tau_c \ll 1$), $T_0 \gg T$ leading to $\Gamma_1^* \propto T^2$. As δ increases, T_0 decreases and the exponential factor tends to disappear. A slowdown in the increase of $\Gamma_1^*(\infty)$ with temperature occurs. Finally, in the strong anharmonicity limit ($\gamma\tau_c \gg 1$), $T_0 \ll T$ and $\Gamma_1^*(\infty)$ becomes a slowly increasing function of the temperature (see figure 6(a)).

Note that the incomplete dephasing–rephasing mechanism shows that vibron scattering in momentum space becomes a real process. Indeed, the phonon decay rate γ represents the finite width of each phonon energy that arises from the phonon–phonon interaction. Therefore, the scattering of a vibron from a wavevector K to a wavevector $K \pm q$ via phonon exchanges becomes possible since energy conservation is required but with an uncertainty of about 2γ. In other words, the phonon anharmonicity opens a relaxation pathway in momentum space that was closed in the harmonic situation. Each vibron eigenstate has a finite lifetime leading to dephasing in real space.

In addition, the vibron–phonon interaction is still responsible for a renormalization of the vibron hopping constant. This effect is accounted for by $\eta(t)$ whose time evolution is easily obtained by inserting (31) and (32) into (35). We have verified that the Debye model provides an analytical expression of $\eta(t)$ in rather good agreement with the numerical results. In particular, $\eta(t)$ first increases for $t < \tau_c$ and then decreases for $\tau_c < t < 2\tau_c$. For $t > 2\tau_c$, it finally converges to

$$\eta(\infty) = \Gamma \frac{(1-e^{-\gamma\tau_c})^2 - 2\gamma\tau_c e^{-\gamma\tau_c}(1-e^{-\gamma\tau_c})}{2\gamma^2\tau_c}. \qquad (41)$$

In the weak anharmonicity limit, $\eta(\infty) \approx -\Gamma\tau_c/2 + \Gamma\gamma\tau_c^2$. It thus increases with δ and exhibits a parabolic dependence on the temperature as shown in figure 6(b). In fact, the anharmonicity favors the increase of $\eta(\infty)$ which becomes positive provided that $\gamma > 0.628\Omega_c$. Nevertheless, $\eta(\infty)$ remains a very small parameter indicating, as expected, that the vibron hopping renormalization can be neglected in the weak coupling limit.

Consequently, after a time of about $2\tau_c$, both $\Gamma_1^*(t)$ and $\eta(t)$ converge to time-independent values and (24) leads to a diffusion coefficient written as

$$D(t) \approx \frac{2\Phi^2(1+\eta(\infty))}{\Gamma_1^*(\infty)}(1-e^{-\Gamma_1^*(\infty)t}). \qquad (42)$$

Whatever δ is, (42) provides a time evolution for $D(t)$ in perfect agreement with the results displayed in figure 7. It shows that the vibrational energy flow results from the competition between the ability of the vibron to delocalize coherently and the coupling with anharmonic phonons responsible for dephasing. Therefore, when the time is shorter than the dephasing time $T_2 = 1/\Gamma_1^*(\infty)$, a coherent energy transfer takes place. The vibron mean square displacement scales as t^2 and $D(t)$ increases linearly according to time. However, as time becomes longer than T_2, the coupling with the phonons induces random fluctuations which destroy the coherent nature of the motion. The vibron quantum state localizes and the vibron realizes random hops between local states mediated by energy exchanges with the bath. This incoherent motion favors the diffusion of the vibrational energy flow so that the vibron mean square displacement scales as $\langle x^2(t)\rangle \approx 2D(\infty)t$. The incoherent diffusion coefficient is thus defined as

$$D(\infty) = \frac{2\Phi^2(1+\eta(\infty))}{\Gamma_1^*(\infty)}. \qquad (43)$$

Since $\eta(\infty)$ is a very small parameter, the behavior of $D(\infty)$ is governed by $\Gamma_1^*(\infty)$. Consequently, as observed in figure 8, $D(\infty)$ scales as $1/\delta^2T^2$ in the weak anharmonicity limit and it diverges when both δ and T tend to zero. As the anharmonicity increases, a slowdown in the decay of $D(\infty)$ with temperature takes place. Finally, in the strong anharmonicity limit, $D(\infty)$ becomes almost temperature-independent. It scales as δ^2, which indicates that the anharmonicity enhances the diffusion.

To conclude this discussion, let us mention that the main result of the present study is to point out the key role played by the spatial correlations in the bath, whether the phonons are harmonic or not. Indeed, in most of the previous works devoted to exciton transport, the dephasing constant usually reduces to $\Gamma_1^*(\infty) = \Gamma_0(\infty)$. It involves the autocorrelation of the site energy only and cross-correlations between neighboring site energies are disregarded (see, for instance, the stochastic transport theory [41] as well as the so-called γ_1 contribution of the Grover–Silbey model [19]). With acoustical harmonic phonons, such approaches completely fail in reproducing the vibron dynamics since they predict dephasing-limited band motion whereas no dephasing occurs. Similarly, with anharmonic phonons, they overestimate the dephasing constant and finally yield the wrong results. For instance, at $T = 310$ K and for $\delta = 10$ nN Å^{-2}, figure 3(b) shows that $\Gamma_0(\infty) = 2.87$ cm^{-1} whereas $\Gamma_1(\infty) = 2.17$ cm^{-1}. Neglecting cross-correlations gives rise to a dephasing time $T_2 = 1.84$ ps whereas our theory predicts $T_2 = 7.57$ ps, i.e. about four times longer. Note that even in the strong anharmonicity limit cross-correlation functions cannot be neglected since (31) and (32) reveal that $\Gamma_0(\infty) \approx 2\Gamma_1(\infty)$. In other words, as previously observed in the strong coupling limit [2], spatial correlations in the phonon bath enhance the dephasing time and allow the observation of the vibron wavelike behavior over a longer time.

6. Conclusion

In this paper, a Davydov model has been used to study the influence of the phonon anharmonicity on the vibron dynamics in a lattice of H-bonded peptide units. To proceed, a TCL-GME for the vibron RDM has been established within the non-adiabatic weak coupling limit. This equation has been used to define the time-dependent diffusion coefficient whose knowledge allows us to understand the way the vibron

propagates along the lattice. It has been shown that the vibron dynamics is governed by the dephasing constant that characterizes how the phonon bath modifies the coherence between neighboring vibron local states. It is defined in terms of the difference between the autocorrelation function of each site energy and the cross-correlation function between neighboring site energies. The behavior of these correlation functions strongly depends on the nature of the phonons and two distinct mechanisms have been identified.

For harmonic phonons, the bath exhibits spatial correlations over an infinite length scale. As a result, the vibron–phonon interaction yields a dephasing–rephasing mechanism in the short time limit which prevents the occurrence of the vibron diffusivity. The vibron propagates freely along the lattice as if it was insensitive to the phonon bath. Keeping its wavelike nature, it induces a coherent vibrational energy flow characterized by a time-dependent diffusion coefficient which increases linearly with time. Note that the short time dephasing–rephasing mechanism defines the counterpart in real space of the virtual phonon emission–absorption mechanism in momentum space which provides an infinite lifetime to each vibron eigenstate.

By contrast, when the anharmonicity is turned on, the phonon–phonon interaction induces a finite lifetime for each phonon mode. Spatial correlations in the bath localize and they occur over a length scale defined as the distance covered by the acoustic wave during their lifetime. Consequently, the rephasing process no longer compensates the dephasing mechanism so that the vibron–phonon coupling tends to destroy the coherent behavior of the vibron. In other words, the phonon anharmonicity opens a relaxation pathway in momentum space so that each vibron eigenstate has a finite lifetime. Dephasing-limited band motion takes place, resulting in a transition between a coherent motion in the short time limit and an incoherent motion in the long time limit. The vibrational energy flow finally diffuses and the corresponding diffusion coefficient scales as $1/T^2$ in the weak anharmonicity limit whereas it becomes a slowly decaying function of the temperature in the strong anharmonicity limit.

To conclude, let us mention that special attention will be paid in forthcoming works to addressing two fundamental questions. First, in the present study, a second-order perturbation theory has been applied to treat the vibron–phonon coupling. At this level of approximation, one-phonon processes contribute to dephasing only when the phonon anharmonicity is included. However, this is no longer the case if high-order processes are taken into account since multi-phonon processes induce dephasing even with harmonic phonons. Consequently, it would be wise to quantify the relevance of high-order processes depending on both the vibron–phonon coupling strength and the phonon anharmonicity. Then, a generalization of the present work will be presented to characterize the vibrational energy flow when two vibrons are excited. In that case, the intramolecular anharmonicity of each amide-I mode acts as a nonlinear source and it favors the occurrence of specific states called two-vibron bound states [4, 42]. These states exhibit an experimental signature within nonlinear pump–probe spectroscopy [43] and they are expected to play a key role for energy storage in proteins due to their formal resemblance to classical breathers.

Appendix. Vibron–phonon coupling correlation function

To evaluate $C_{x_1,x_2}(t)$, we apply the single-mode relaxation-time method in which one calculates the phonon mode q lifetime by assuming that all the other modes form a bath in thermal equilibrium [29]. To proceed, (3) is rewritten as

$$H_{\mathrm{p}} = \sum_q \Omega_q a_q^\dagger a_q + \sum_q S_q a_q^\dagger + S_q^\dagger a_q \tag{A.1}$$

where S_q is the coupling strength between the mode q and the remaining phonons as

$$S_q = \sum_{q_1 q_2} \sum_{\sigma_1 \sigma_2} \frac{\lambda(q, q_1, q_2)}{\sqrt{N}} \sigma_1 \sigma_2 \delta_{q+\sigma_1 q_1+\sigma_2 q_2} a_{q_1}^{\sigma_1} a_{q_2}^{\sigma_2}. \tag{A.2}$$

In (A.2), $\sigma_i = \pm 1$, $a_q^{+1} \equiv a_q^\dagger$, $a_q^{-1} \equiv a_q$ and δ_K is the periodic Kronecker symbol in the space of the reciprocal lattice. The term $\lambda(q, q_1, q_2)$ is defined as

$$\lambda(q, q_1, q_2) = -\frac{4\mathrm{i}\delta}{3\hbar}\left(\frac{\hbar}{2M}\right)^{3/2} \frac{\sin(\frac{q}{2})\sin(\frac{q_1}{2})\sin(\frac{q_2}{2})}{\sqrt{\Omega_q \Omega_{q_1} \Omega_{q_2}}}. \tag{A.3}$$

Then, a projector method is used to evaluate the time evolution of the phonon operator correlation functions. By performing a second-order expansion with respect to S_q, it is shown that the phonons still behave as independent bosons. Nevertheless, it is as if each mode was characterized by a complex eigenfrequency $\Omega_q \pm \mathrm{i}\gamma_q$, where γ_q is the so-called phonon decay rate. The reduced dimensionality of the 1D lattice provides particular properties. The decay rate is thus q-independent, and its expression, whatever the temperature, corresponds to its high temperature limit [26–28] as

$$\gamma = \frac{k_{\mathrm{B}} T}{4} \frac{\delta^2}{W^3} \Omega_{\mathrm{c}}. \tag{A.4}$$

In that context, from (4), $C_{x_1,x_2}(t)$ is finally written as

$$C_{x_1 x_2}(t) = K(|x_1 - x_2|, t) - \mathrm{i}S(|x_1 - x_2|, t) \tag{A.5}$$

where $K(x, t)$ and $S(x, t)$ are defined as

$$K(x,t) = \frac{2E_{\mathrm{B}}}{N} \sum_q \coth(\Omega_q / 2k_{\mathrm{B}}T)\Omega_q \times \cos^2\left(\frac{q}{2}\right)\cos(\Omega_q t - qx)\mathrm{e}^{-\mathrm{i}\gamma t} \tag{A.6}$$

$$S(x,t) = \frac{2E_{\mathrm{B}}}{N} \sum_q \Omega_q \cos^2\left(\frac{q}{2}\right)\sin(\Omega_q t - qx)\mathrm{e}^{-\mathrm{i}\gamma t}.$$

References

[1] Pouthier V and Tsybin Y O 2008 *J. Chem. Phys.* **129** 095106
[2] Pouthier V 2008 *Phys. Rev.* E **78** 061909
[3] Pouthier V 2007 *Phys. Rev.* E **75** 061910
[4] Pouthier V 2008 *Physica* D **237** 106

[5] Pouthier V 2006 *Physica* D **221** 13
[6] Davydov A S and Kisluka N I 1973 *Phys. Status Solidi* **59** 465
Davydov A S and Kisluka N I 1976 *Zh. Eksp. Teor. Fiz* **71** 1090
Davydov A S and Kisluka N I 1976 *Sov. Phys.—JETP* **44** 571 (Engl. Transl.)
[7] Scott A C 1982 *Phys. Rev.* A **26** 578
[8] Scott A C 1992 *Phys. Rep.* **217** 1
[9] Forner W 1997 *Int. J. Quantum Chem.* **64** 351
[10] Scott A C 2003 *Nonlinear Science* (Oxford: Oxford University Press)
[11] Brown D W and Ivic Z 1989 *Phys. Rev.* B **40** 9876
[12] Brown D W, Lindenberg K and Wang X 1990 *Davydov's Soliton Revisited* (New York: Plenum) p 63
[13] Ivic Z, Kapor D, Skrinjar M and Popovic Z 1993 *Phys. Rev.* B **48** 3721
[14] Ivic Z, Kostic D, Przulj Z and Kapor D 1997 *J. Phys.: Condens. Matter* **9** 413
[15] Tekic J, Ivic Z, Zekovic S and Przulj Z 1999 *Phys. Rev.* E **60** 821
[16] Przulja Z, Cevizovic D, Zekovic S and Ivic Z 2008 *Chem. Phys. Lett.* **462** 213
[17] Lang I G and Firsov Yu A 1962 *Sov. Phys.—JETP* **16** 1293
[18] Yarkony D and Silbey R 1976 *J. Chem. Phys.* **65** 1042
[19] Grover M and Silbey R 1971 *J. Chem. Phys.* **54** 4843
[20] Silbey R and Munn R W 1979 *J. Chem. Phys.* **72** 2763
[21] Capek V and Barvik I 1987 *J. Phys. C: Solid State Phys.* **20** 1459
[22] Dolderer H and Wagner M 1998 *J. Chem. Phys.* **108** 261
[23] Kuprievich V A 1990 *Davydov Soliton Revisited* (New York: Plenum) p 199
[24] Pierce B M 1990 *Davydov Soliton Revisited* (New York: Plenum) p 209
[25] Ostergard N 1990 *Davydov Soliton Revisited* (New York: Plenum) p 229
[26] Maradudin A A and Fein A E 1962 *Phys. Rev.* **128** 2589
[27] Pathak N K 1965 *Phys. Rev.* **139** A1569
[28] Freidkin E S, Horton G K and Cowley E R 1995 *Phys. Rev.* B **52** 3322
Freidkin E S, Horton G K and Cowley E R 1996 *J. Phys.: Condens. Matter* **8** 8497
[29] Srivastava G P 1990 *The Physics of Phonons* (New York: Hilger)
[30] Shibata F, Takahashi Y and Hashitsume N 1977 *J. Stat. Phys.* **17** 171
[31] Uchiyama C and Shibata F 1999 *Phys. Rev.* E **60** 2636
[32] Breuer H P and Kappler B 2001 *Ann. Phys.* **291** 36
[33] Breuer H P, Kappler B and Petruccione F 1999 *Phys. Rev.* A **59** 1633
[34] Breuer H P, Gemmer J and Michel M 2006 *Phys. Rev.* E **73** 016139
[35] Schroder M, Kleinekathofer U and Schreiber M 2006 *J. Chem. Phys.* **124** 084903
[36] Esposito M and Gaspard P 2005 *Phys. Rev.* B **71** 214302
[37] Kubo R 1969 *Adv. Chem. Phys.* **15** 101
[38] Sonnek M and Wagner M 1992 *J. Chem. Phys.* **97** 5037
[39] Sonnek M and Wagner M 1996 *Phys. Rev.* B **54** 9213
[40] d'Ovidio F, Bohr H G and Lindgard P A 2005 *Phys. Rev.* E **71** 026606
[41] Reineker P 1982 *Exciton Dynamics in Molecular Crystals and Aggregates* (Berlin: Springer)
[42] Falvo C and Pouthier V 2005 *J. Chem. Phys.* **123** 184710
[43] Edler J, Pfister R, Pouthier V, Falvo C and Hamm P 2004 *Phys. Rev. Lett.* **93** 106405